

1 **Taxonomic revision of genus *Carinolithus* (Early - Middle Jurassic) based on morphometric**  
2 **analyses and diagenesis observations: implications for biostratigraphy and evolutionary trends.**

3 Stefano Visentin<sup>a</sup>, Giulia Faucher<sup>a</sup>, Emanuela Mattioli<sup>b, c</sup>, Elisabetta Erba<sup>a</sup>

4 <sup>a</sup> Dipartimento di Scienze della Terra, Università degli Studi di Milano, Via Mangiagalli 34, 20133  
5 Milano, Italy ([stefano.visentin@unimi.it](mailto:stefano.visentin@unimi.it); [giulia.faucher@unimi.it](mailto:giulia.faucher@unimi.it); [elisabetta.erba@unimi.it](mailto:elisabetta.erba@unimi.it)).

6 <sup>b</sup> Univ Lyon, Univ Lyon 1, ENSL, CNRS, LGL-TPE, F-69622, Villeurbanne, France

7 <sup>c</sup> Institut Universitaire de France (IUF) ([emanuela.mattioli@univ-lyon1.fr](mailto:emanuela.mattioli@univ-lyon1.fr)).

8 **Corresponding author** : Stefano Visentin, [stefano.visentin@unimi.it](mailto:stefano.visentin@unimi.it). Dipartimento di Scienze della  
9 Terra, Università degli Studi di Milano, Via Mangiagalli 34, 20133 Milano, Italy.

10

11 **Abstract**

12 We applied morphometric analyses performed with a polarizing light microscope on a total of 100  
13 specimens of *Carinolithus superbus* and *C. magharensis* to clarify the taxonomy based on  
14 measurements of total height (TH), stem height (SH), stem width (SW), proximal shield width (PS),  
15 distal shield width (DS) and thickness of the distal shield (TDS). Statistical analyses showed that  
16 three of these parameters, namely the DS, TDS and SW, are diagnostic for taxa discrimination. New  
17 taxa include *C. superbus* subsp. *crassus* subsp. nov. and *C. magharensis* subsp. *minor* subsp. nov.  
18 Specimens of *C. cantaluppii* were qualitatively investigated to assess the potential role of secondary  
19 modifications and our results revealed that, indeed, *C. cantaluppii* is a diagenetic artefact due to  
20 different degrees of overgrowth on specimens of *C. poulabronei*, *C. superbus* subsp. *crassus*, *C.*  
21 *superbus* subsp. *superbus*, *C. magharensis* subsp. *minor* and *C. magharensis* subsp. *magharensis* .  
22 This implies that *C. cantaluppii* is not a true taxon, and the overgrowth phase of *Carinolithus*  
23 specimens is an effective proxy to assess the diagenetic degree. The morphometry-based revised  
24 taxonomy of the genus *Carinolithus* was applied to improve the biostratigraphic resolution of the  
25 Toarcian-Aalenian interval, with further implications for the reconstruction of evolutionary trends.

26

27 **Keywords**

28 Calcareous nannofossils; Early-Middle Jurassic; *Carinolithus*; Morphometry; Taxonomy; Diagenesis

29

30 **1. Introduction**

31 The genus *Carinolithus* was initially established as *Rhabdolithus* by Deflandre in Deflandre & Fert  
32 (1954) and, in the same work, the new species *R. sceptrum*, *R. superbus* and *R. clavatus* (Fig. 1) were  
33 introduced. Later, Prins in Grün et al. (1974) established the genus *Carinolithus* and emended *R.*  
34 *superbus* as *C. superbus*. Similarly, Medd (1979) emended *R. sceptrum* and *R. clavatus* as *C.*  
35 *sceptrum* and *C. clavatus*, respectively. Bown (1987a) interpreted *C. sceptrum* as a variant of *C.*  
36 *superbus* and considered *C. clavatus* to group incomplete specimens of *C. superbus* without the distal  
37 shield. Consequently, the species *C. clavatus* and *C. sceptrum* were abandoned by subsequent authors.

38 The species *C. magharensis* was initially established within the genus *Hexalithus* (Moshkovitz &  
39 Ehrlich, 1976) and later Bown (1987a) moved it to genus *Carinolithus* based on scanning electron  
40 microscope investigations since the hexaliths are distal shields of carinolithids. According to Bown  
41 (1987a), *C. superbus* and *C. magharensis* are easily discriminated if detected in distal view (DV) as  
42 the number of wedge-shaped elements forming their distal shields is ten to twelve in *C. superbus* and  
43 six in *C. magharensis*. Moreover, Bown (1987a) observed that the distal shield of *C. magharensis*  
44 flares sharply (roughly at right angles) from the stem and has a rectangular shape in a transverse  
45 section whereas that of *C. superbus* flares more gradually. Taxonomic incongruity, however, emerges  
46 when *Carinolithus* coccoliths are observed in side view (SV), because the shape is essentially the  
47 same (T-shape structure). Two additional species were established: *C. cantaluppii* by Cobiauchi  
48 (1990) and *C. poulabronei* by Mattioli (1996). The latter possesses a peculiar V-shape structure in  
49 SV and is, thus, easily distinguishable from *C. superbus* and *C. magharensis*.

50 A solid taxonomy is fundamental since the different species of this genus are used as events in  
51 standard zonations of higher (Bown, 1987a; Bown et al., 1988; Bown & Cooper, 1998; Fraguas et al.,  
52 2015) and lower latitudes (Mattioli & Erba, 1999; Ferreira et al., 2019). In particular, the first

53 occurrence (FO) of *C. superbus* marks the inception of the NJT6 and NJ6 Zones in the Tethyan and  
54 Boreal Realms, respectively, and is calibrated with the positive carbon isotope rebound preceding the  
55 negative carbon isotope excursion which is correlative to the Toarcian Oceanic Anoxic event (T-  
56 OAE) on a supraregional scale (Mattioli et al., 2004; 2013; Casellato & Erba, 2015; Ferreira et al.,  
57 2019). The FO of *C. magharensis* is used to define the base of the NJT8f Subzone (Ferreira et al.,  
58 2019), which corresponds to the basal Aalenian Opalinum Zone. Moreover, although not considered  
59 zonal/subzonal events, the FOs of *C. cantaluppii* and *C. poul nabroni* are indicated as additional  
60 biohorizons in the standard biozonations.

61 In this work morphometric analyses, performed on smear slides under a polarizing light microscope,  
62 were applied to *C. superbus* and *C. magharensis* specimens in order to clarify the taxonomy.  
63 Moreover, a detailed study of *C. cantaluppii* was conducted to ascertain the potential role of  
64 overgrowth on its morphology.

65 *Fig. 1, about here, one column and half.*

66

## 67 **2. Materials and Methods**

68 A total of 100 specimens of the *C. superbus* and *C. magharensis* groups were investigated for  
69 morphometric analyses using photographs taken with polarizing light microscope. A total of 62  
70 images were selected from published works (Appendix 1) complemented with 38 additional  
71 specimens from sections in the Lombardy Basin (Sogno Core in northern Italy and Breggia section  
72 in southern Switzerland). In Appendix 1, for each investigated specimen the following information  
73 (as reported in the original paper) is given: calcareous nanofossil Zones/Subzones, ammonite  
74 Zones/Subzones, stage/substage, core/section.

75 Smear slides were prepared with the random settling technique (Geisen et al., 1999) for the Sogno  
76 Core and the standard smear slide technique (Bown & Young, 1998) for the Breggia section.  
77 Photographs were acquired using a Leitz Laborlux optical polarizing light microscope at 1250X  
78 magnification and a Q imaging Micropublisher 5.0. RTV digital camera. Images were analyzed using

79 a PC with Q-capture Pro suite software adapted for nannofossil analyses. Measurements were taken  
80 using ImageJ software, with an error of measurements of  $\pm 0.08 \mu\text{m}$ .

81 Six parameters were measured: the Total Height (TH); the Stem Height (SH); the Stem Width (SW);  
82 the Proximal Shield diameter (PS); the Distal Shield diameter (DS) and the Thickness of the Distal  
83 Shield (TDS) as illustrated in Fig. 2. In case of observations in side view or when specimens are  
84 broken or heavily overgrown, a few parameters could not be measured. A total of 341 measurements  
85 were obtained: 29 for the TH, 29 for the SH, 75 for the SW, 29 for the PS, 100 for the DS, 79 for the  
86 TDS.

87 Statistical parameters like mean, mode, median, standard deviation and 95% confidence level were  
88 calculated using the Matlab and PAST softwares and reported in Tab. 1. Moreover, a mixture analysis  
89 was run, using PAST software (Hammer et al., 2001), in order to find the overall mixing proportions  
90 of specimens belonging to different taxa. This probabilistic model is a maximum-likelihood method  
91 for estimating the parameters (mean, standard deviation and proportion) of two or more univariate  
92 normal distributions, based on a pooled univariate sample (Hammer & Harper, 2006).

93 As far as *C. cantaluppii* is concerned, 50 specimens were qualitatively investigated taking four  
94 pictures of each specimen, both with and without quartz lamina, both at  $0^\circ$  and  $45^\circ$  to the polarizers.

95 *Fig. 2, about here, two columns.*

96

### 97 **3. Results**

98 Figure 2 synthesizes the results obtained for TH, SH, SW, PS, DS and TDS for *C. superbus* (blue)  
99 and *C. magharensis* (red) specimens. Based on the DS and TDS two different-sized groups of  
100 coccoliths are distinguished. As far as the DS is concerned, one group shows values ranging from 2.8  
101 to  $6.8 \mu\text{m}$  whereas the other is from  $7.8$  to  $10.9 \mu\text{m}$ . The bigger-sized group comprises only specimens  
102 of the *C. magharensis* group whereas the smaller-sized coccoliths belong to both groups. We also  
103 notice that no specimens have a DS in the range of  $6.9$  to  $7.7 \mu\text{m}$ .

104 The TDS separates a first group varying between 0.4 and 1.5  $\mu\text{m}$  from a second one in the range of  
105 1.8 - 2.9  $\mu\text{m}$ . This latter bigger-sized group entirely consists of specimens of the *C. magharensis*  
106 group while the smaller-sized only comprises specimens of the *C. superbis* group.

107 The parameters TH, SH, SW and PS do not discriminate between the *C. superbis* and *C. magharensis*  
108 groups. Nevertheless, *C. magharensis* specimens generally show higher values of TH and SH. Mode,  
109 median, mean and standard deviation are provided in Tab. 1 for each parameter by considering a) all  
110 the investigated specimens; b) specimens of the *C. magharensis* group; c) specimens of the *C.*  
111 *superbis* group. Both DS and TDS have mode, median, mean and standard deviation much higher  
112 (almost double) in the *C. magharensis* group, thus showing systematic differences.

113 *Tab. 1, about here, one column and half.*

114 The Pearson's correlation coefficient (Fig. 3) shows: a) positive values for TH/SH, TH/DS, TH/TDS,  
115 SH/PS, SH/DS, SH/TDS, SW/PS, SW/DS, PS/DS, DS/TDS and b) negative coefficients for TH/SW,  
116 TH/PS, SH/SW, SW/TDS, PS/TDS. In particular, a strong positive correlation exists for TH/SH ( $r =$   
117  $0.97$ ), DS/TH ( $r = 0.69$ ), TDS/TH ( $r = 0.66$ ), DS/SH ( $r = 0.62$ ), TDS/SH ( $r = 0.51$ ), TDS/DS ( $r =$   
118  $0.64$ ).

119 The Pearson's correlation coefficient was also calculated separately for the *C. magharensis* and *C.*  
120 *superbis* specimens: a clear distinction between the two groups is indicated only for the TH/TDS,  
121 SH/TDS, SW/TDS, PS/TDS, and DS/TDS ratios, as evidenced by the red and blue clouds in Fig. 3.

122 *Fig. 3, about here, two columns.*

123

## 124 **4. Discussion**

### 125 **4.1. Taxonomic revision of *C. superbis* and *C. magharensis***

126 Morphometric analyses turned out to be an excellent tool to separate *C. magharensis* and *C. superbis*  
127 specimens. In particular, the DS (Fig. 4a) discriminates 23 specimens with sizes of 7.8 - 10.9  $\mu\text{m}$   
128 from a group of 77 specimens with a DS ranging between 2.8 and 6.8  $\mu\text{m}$ . The former group  
129 comprises exclusively large *C. magharensis* specimens, whereas the second group includes *C.*

130 *superbus* coccoliths and small specimens of *C. magharensis*. Within this latter group, the TDS  
131 separates two clusters (Fig. 4b): one cluster includes 56 specimens characterized by a TDS ranging  
132 from 0.4 to 1.5  $\mu\text{m}$  and a second one, grouping 18 specimens, with a TDS varying from 1.8 to 2.9  
133  $\mu\text{m}$ . The latter group consists exclusively of *C. magharensis* with a thicker distal shield relative to *C.*  
134 *superbus* specimens.

135 A further subdivision was obtained using the SW of *C. superbus* specimens (Fig. 4c): a group includes  
136 30 specimens characterized by a SW spanning from 0.5 to 1.0  $\mu\text{m}$  and another cluster of 26 coccoliths  
137 with a SW varying from 1.3 to 2.5  $\mu\text{m}$ . Therefore, within *C. superbus*, the SW separates thin from  
138 thick morphotypes.

139 *Fig. 4, about here, two columns.*

140 Our morphometric analyses allowed the identification of four separate groups: large *C. magharensis*  
141 ( $\text{DS} \geq 7.8 \mu\text{m}$ ), small *C. magharensis* ( $\text{DS} \leq 6.8 \mu\text{m}$  and  $\text{TDS} \geq 1.8 \mu\text{m}$ ), thin *C. superbus* ( $\text{SW} \leq 1$   
142  $\mu\text{m}$ ,  $\text{TDS} < 1.5 \mu\text{m}$  and  $\text{DS} < 6.8 \mu\text{m}$ ) and thick *C. superbus* ( $\text{SW} \geq 1.3 \mu\text{m}$ ,  $\text{TDS} \leq 1.5 \mu\text{m}$  and  $\text{DS}$   
143  $< 6.8 \mu\text{m}$ ).

144 The large *C. magharensis* specimens ( $\text{DS} \geq 7.8 \mu\text{m}$ ) are characterized by DS fully consistent with the  
145 holotype of *H. magharensis* possessing a DS of 8  $\mu\text{m}$ , whereas the small *C. magharensis* specimens  
146 ( $\text{DS} \leq 6.8 \mu\text{m}$ ) evidently do not fall within the original definition of this taxon. Therefore, the two  
147 morphogroups can be distinguished as *C. magharensis* subsp. *magharensis* (large specimens) and *C.*  
148 *magharensis* subsp. *minor* subsp. nov. (small specimens; see taxonomic remarks later on).

149 Within the *C. superbus* group, the thin specimens ( $\text{SW} \leq 1.0 \mu\text{m}$ ) are consistent with the original  
150 description of this species. In fact, the holotype of *R. superbus* (Deflandre *in* Deflandre & Fert, 1954;  
151 figs. 24, 25) has a SW of 0.7  $\mu\text{m}$ . The specimens with  $\text{SW} \geq 1.3 \mu\text{m}$ , instead, are distinctly thicker.  
152 Accordingly, the two morphogroups can be distinguished as *C. superbus* subsp. *superbus* (thin  
153 specimens) and *C. superbus* subsp. *crassus* subsp. nov. (thick specimens; see taxonomic remarks later  
154 on).

155 Recently, Ferreira et al. (2019) documented *C. superbus* specimens characterized by a thinner and  
156 longer stem which they named “*C. superbus* thin and long”; also, they made a distinction between *C.*  
157 *magharensis* and “*C. magharensis* large”. The qualitative taxonomic subdivision of Ferreira et al.  
158 (2019) is consistent with our morphometric results and, specifically, their *C. superbus* corresponds  
159 to *C. superbus* subsp. *crassus*, *C. superbus* “thin and long” to *C. superbus* subsp. *superbus*, *C.*  
160 *magharensis* to *C. magharensis* subsp. *minor*, and *C. magharensis* “large” to *C. magharensis* subsp.  
161 *magharensis*. Figure 5 summarizes the morphometric data of the holotypes and specimens analyzed  
162 in this work for *C. superbus* subsp. *crassus*, *C. superbus* subsp. *superbus*, *C. magharensis* subsp.  
163 *minor* and *C. magharensis* subsp. *magharensis*. Polarizing light microscope photos are presented in  
164 Fig. 6. Based on morphometric investigations, we established size-dependent new taxa.

165 *Fig. 5, about here, one columns and half.*

166 In the following section, the systematics of *C. superbus* subsp. *crassus*, *C. superbus* subsp. *superbus*,  
167 *C. magharensis* subsp. *minor* and *C. magharensis* subsp. *magharensis* are detailed. Diagnosis,  
168 description, remarks and differentiation are provided for each taxon.

169

170 Genus *Carinolithus* Prins in Grün et al. (1974)

171 *Carinolithus superbus* subsp. *crassus* Visentin & Erba subsp. nov.

172 Fig. 6, a-f; Fig. 8, c1-c7, d1-d6.

173 **Etymology:** the name derives from the diagnostic thick stem.

174 **Diagnosis:** a subspecies of *Carinolithus superbus* with a thick stem (width > 1 µm).

175 **Description:** this new subspecies is characterized morphometrically by possessing a stem width > 1  
176 µm and a relatively narrow but still open axial canal.

177 **Remarks:** on the basis of available data the total height varies between 6.3 – 12.1 µm; stem width:  
178 1.3 – 2.5 µm; proximal shield diameter: 2.1 – 3.9 µm; distal shield diameter: 3.0 – 5.6 µm; thickness  
179 of distal shield: 0.4 – 1.5 µm.

180 **Stratigraphic range:** FO in the Lower Toarcian, Polymorphum or Tenuicostatum ammonite Zone,  
181 correlative with the positive carbon isotope rebound preceding the negative carbon isotope excursion  
182 which is correlative to the Toarcian Oceanic Anoxic event (T-OAE). The FO of this subspecies  
183 substitutes the FO of *C. superbus* as a marker for the base of the NJT6 and NJ6 Zones.

184 **Differentiation:** *Carinolithus superbus* subsp. *crassus* differs from *C. superbus* subsp. *superbus* by  
185 its thicker stem (width > 1 µm) and by its wider and well distinguishable axial canal, from *C.*  
186 *poulnabronei* by its T- shape, from *C. magharensis* subsp. *minor* by its thinner distal shield (≤ 1.5  
187 µm) and from *C. magharensis* subsp. *magharensis* by its thinner (≤ 1.5 µm) and smaller (< 6 µm)  
188 distal shield. The T-shape of *C. superbus* subsp. *crassus* is unambiguously different for the V-shape  
189 of *C. poulnabronei*.

190 **Holotype:** Fig. 8, c1-c4. Holotype total height: 8.8 µm; stem width: 1.7 µm; proximal shield diameter  
191 3.1 µm; distal shield diameter: 4.6 µm; thickness of the distal shield: 1.3 µm.

192 **Type locality:** Colle di Sogno (Italy).

193 **Type level:** Jurassic, Toarcian.

194 **Depository:** Department of Earth Sciences “Ardito Desio” of Milan (Reference MPUM 1870).

195

196 *Carinolithus superbus* (Deflandre in Deflandre & Fert, 1954) Prins in Grün et al. (1974)

197 subsp. *superbus* emend. Visentin & Erba

198 Fig. 6, g-l; Fig. 8, e1-e8, f1-f6.

199 **Basionym:**

200 1954 *Rhabdolithus superbus* Deflandre in Deflandre & Fert, p. 160; pl. 15; figs. 24-25; text-fig. 93.

201 **Reference:**

202 1974 *Carinolithus superbus* Deflandre; Prins in Grün et al., p. 313; pl. 15; figs. 1-3; text-fig. 13.

203 **Description:** the original description of *Carinolithus superbus* by Deflandre in Deflandre & Fert  
204 (1954) is maintained for *Carinolithus superbus* subsp. *superbus*. This subspecies is further  
205 characterized morphometrically by possessing a stem width ≤ 1 µm.



206 **Remarks:** on the basis of available data the total height varies between 5.8 – 15.9  $\mu\text{m}$ ; stem width:  
207 0.5 – 1.0  $\mu\text{m}$ ; proximal shield diameter: 1.4 – 3.9  $\mu\text{m}$ ; distal shield diameter: 3.0 – 5.6  $\mu\text{m}$ ; thickness  
208 of distal shield: 0.4 – 1.5  $\mu\text{m}$ .

209 **Stratigraphic range:** FO between the uppermost part of the Levisoni Zone and the base of the  
210 Bifrons Zone (Ferreira et al., 2019; Lower/Middle Toarcian boundary), in the lowermost part of the  
211 NJT7 and NJ7 Zones.

212 **Differentiation:** *Carinolithus superbus* subsp. *superbus* differs from *C. superbus* subsp. *crassus* by  
213 its thinner stem ( $\leq 1 \mu\text{m}$ ), from *C. poulnabronei* by its T- shape, from *C. magharensis* subsp. *minor*  
214 by its thinner distal shield ( $\leq 1.5 \mu\text{m}$ ) and from *C. magharensis* subsp. *magharensis* by its thinner ( $\leq$   
215 1.5  $\mu\text{m}$ ) and smaller ( $< 6 \mu\text{m}$ ) distal shield.

216 **Holotype:** Deflandre in Deflandre & Fert (1954; figs. 24-25). Holotype total height: 10.3  $\mu\text{m}$ ; stem  
217 width: 0.7  $\mu\text{m}$ ; proximal shield diameter: 2.7  $\mu\text{m}$ ; distal shield diameter: 4.3  $\mu\text{m}$ ; thickness of the  
218 distal shield: 1.0  $\mu\text{m}$ .

219 **Type locality:** Villers-sur-Mer, Calvados (Spain) (Deflandre & Fert, 1954).

220 **Type level:** Jurassic, Oxfordian (Deflandre & Fert, 1954).

221 **Depository:** Collection du Laboratoire de Micropaléontologie de l'Ecole pratique des Hautes Etudes,  
222 Paris (Deflandre & Fert, 1954).

223

224 *Carinolithus magharensis* subsp. *minor* Visentin & Erba subsp. nov.

225 Fig. 6, m-r; Fig. 8, g1-g7, h1-h4.

226 **Etymology:** the name derives from the diagnostic small diameter of the distal shield relative to *C.*  
227 *magharensis* subsp. *magharensis*.

228 **Diagnosis:** a subspecies of *C. magharensis* with a thick ( $> 1.5 \mu\text{m}$ ) and small ( $< 7 \mu\text{m}$ ) distal shield.  
229 The distal shield is constituted by 6 elements.

230 **Description:** this new subspecies is characterized morphometrically by possessing a thickness of the  
231 distal shield  $> 1.5 \mu\text{m}$  and a distal shield diameter  $< 7 \mu\text{m}$  which is constituted by 6 elements.

232 **Remarks:** on the basis of available data the total height varies between 11.1 – 16.6  $\mu\text{m}$ ; stem width:  
233 0.6 – 1.1  $\mu\text{m}$ ; proximal shield diameter: 1.7 – 3.0  $\mu\text{m}$ ; distal shield diameter: 4.1 – 6.8  $\mu\text{m}$ ; thickness  
234 of distal shield: 1.8 – 2.9  $\mu\text{m}$ . Morphometric analyses separate specimens with distal shield  $\leq 6.8 \mu\text{m}$   
235 from specimens  $\geq 7.8 \mu\text{m}$  (*C. magharensis* subsp. *magharensis*) and no intermediate sizes have been  
236 found. According to the morphometric diagnosis of *C. magharensis* subsp. *minor*, specimens  
237 attributed to *C. magharensis* by Bown (1987a; page 59) show features (distal shield diameter varying  
238 between 4.5 and 5.9  $\mu\text{m}$ ) consistent with *C. magharensis* subsp. *minor*.

239 **Stratigraphic range:** *Hexalithus magharensis* was reported from the late Opalinum Zone (Early  
240 Aalenian) in the Tethyan Realm occurring shortly after *Watznaueria contracta* (Mattioli & Erba,  
241 1999). Recent data from the well-dated Cabo Mondego section (Portugal) show an earlier occurrence  
242 of *C. magharensis*, close to the base of the Opalinum ammonite Zone still shortly following the FO  
243 of *W. contracta* reported from the basal Aalensis ammonite Zone of latest Toarcian age (Ferreira et  
244 al., 2019). Because of its distinctive morphological characters, the FO of *C. magharensis* was  
245 proposed to define the base of the NJT8f Subzone (Ferreira et al., 2019). The separation of the two  
246 subspecies *C. magharensis* subsp. *minor* and *C. magharensis* subsp. *magharensis* implies that future  
247 investigations will clarify their FOs.

248 **Differentiation:** *Carinolithus magharensis* subsp. *minor* differs from *C. magharensis* subsp.  
249 *magharensis* for its smaller distal shield ( $< 7 \mu\text{m}$ ), from *C. superbus* subsp. *crassus* and *C. superbus*  
250 subsp. *superbus* for its thicker distal shield ( $> 1.5 \mu\text{m}$ ).

251 **Holotype:** Fig. 8, g1-g4. Holotype distal shield diameter: 5.6  $\mu\text{m}$ ; thickness of the distal shield: 2.3  
252  $\mu\text{m}$ .

253 **Type locality:** Breggia (Switzerland).

254 **Type level:** Jurassic, Aalenian.

255 **Depository:** Department of Earth Sciences “Ardito Desio” of Milan (Reference MPUM 1869).

256

257 *Carinolithus magharensis* (Moshkovitz & Ehrlich, 1976) Bown (1987a) subsp. *magharensis* emend.

258 Visentin & Erba

259 Fig. 6, s-x; Fig. 8, i1-i6.

260 Basionym:

261 1976 *Hexalithus magharensis* Moshkovitz & Ehrlich, p. 16, pl. 8; figs. 12-15.

262 Reference:

263 1987a *Carinolithus magharensis* Moshkovitz & Ehrlich; Bown, pp. 58-59; pl. 8; figs. 4-6; pl. 14;  
264 figs. 17-20.

265 **Description:** the original description of Moshkovitz & Ehrlich (1976) is maintained for specimens  
266 observed in top view. This subspecies is further characterized by a thick ( $> 1.5 \mu\text{m}$ ) and large ( $\geq 8$   
267  $\mu\text{m}$ ) distal shield constituted by 6 elements. The original description of *Hexalithus magharensis*  
268 applies to hexaliths more or less hexagonal in shape composed of 6 distinct triangular elements;  
269 towards the margin, the corners of these triangles are obliquely truncated. In light microscope each  
270 element has its own optical orientation. *Hexalithus magharensis* comprises specimens of 8-9  $\mu\text{m}$  in  
271 diameter. Bown (1987a) emended *H. magharensis* by transferring the species into the genus  
272 *Carinolithus*. However, the illustrated specimens possess a distal shield diameter varying between  
273 4.5 and 5.9  $\mu\text{m}$ , thus definitively smaller than the holotype and species variability of *H. magharensis*.  
274 Our morphometric analyses confirm the separation of two groups, and we attribute to *C. magharensis*  
275 subsp. *magharensis* only specimens with a distal shield larger than 8  $\mu\text{m}$ .

276 **Remarks:** the original description of Moshkovitz & Ehrlich (1976) is confirmed for specimens  
277 observed in top views. On the basis of available data, the stem width varies between 1.2 – 1.7  $\mu\text{m}$ ;  
278 distal shield diameter: 7.8 – 10.9  $\mu\text{m}$ ; thickness of distal shield: 2.0 – 2.9  $\mu\text{m}$ .

279 **Stratigraphic range:** Although *C. magharensis* subsp. *minor* and *C. magharensis* subsp.  
280 *magharensis* are very rare after their first occurrence (i.e., 1-2 specimens in 250 fields of view at 1250  
281 X magnification), a re-analysis of the Cabo Mondego section shows the presence of both subspecies

282 from the Early Aalenian (base Opalinum Zone). However, *C. magharensis* subsp. *magharensis*  
283 becomes more common from the Bajocian upwards.

284 **Differentiation:** *Carinolithus magharensis* subsp. *magharensis* differs from *C. magharensis* subsp.  
285 *minor* for its larger distal shield ( $> 8 \mu\text{m}$ ) and more sharply truncated triangular elements.

286 **Holotype:** Moshkovitz & Ehrlich (1976, figs. 14-15). Holotype distal shield diameter:  $8 \mu\text{m}$ .

287 **Type locality:** Israel. This species occurs in the Gebel Maghara outcrop, in the Lower Sherif and  
288 Upper Daya Formations (Moshkovitz & Ehrlich, 1976).

289 **Type level:** Jurassic, Bajocian-Bathonian (Moshkovitz & Ehrlich, 1976).

290 **Depository:** Geological Survey of Israel (Moshkovitz & Ehrlich, 1976).

291 *Fig. 6, about, here, two columns.*

292

#### 293 **4.2. Effects of diagenesis on the genus *Carinolithus***

294 The taxon *C. cantaluppii* was established by Cobianchi (1990; fig. 4, h) as a species of *Carinolithus*  
295 with a small proximal shield and a large distal spine that typically broadens at about  $\frac{1}{4}$  (from the base)  
296 maintaining the size (width) up to the distal shield. Under crossed nicols *C. cantaluppii* shows high  
297 birefringence colors (from white to orange) and a clear extinction line in the middle of the spine. The  
298 proximal shield diameter is  $2.3\text{-}2.8 \mu\text{m}$ , the distal shield diameter is  $3.0\text{-}4.0 \mu\text{m}$ , and the height is  $8.0\text{-}$   
299  $10 \mu\text{m}$ . Cobianchi (1990) used the term “spine” as the equivalent of “stem” and, therefore, the  
300 “broadening of the spine” corresponds to the broadening of the stem. Based on the original  
301 description, *C. cantaluppii*, similarly to other *Carinolithus* species, should have a symmetric shape  
302 including the broadening of the stem. However, the only specimen (presumably the holotype)  
303 illustrated by Cobianchi (1990) is clearly asymmetric as the two sides of the stem broaden at different  
304 points and with different widths. The right side of the stem (Fig. 1e) broadens at about  $\frac{1}{4}$  from the  
305 base (as provided by the author’s description) whereas the left side of the stem slightly broadens (less  
306 wide and with a different shape) at about  $\frac{1}{2}$  from the base. The drawing of *C. cantaluppii* in Mattioli  
307 (1996; fig. 3) shows a symmetric stem broadening at about  $\frac{3}{4}$  from the base. In the literature, several

308 photos of *C. cantaluppii* specimens show an extremely asymmetric shape (e.g. Cobianchi 1990, fig.  
309 4, h; Cobianchi 1992, fig. 20, g; Perilli & Duarte, 2006, pl. 1, fig. 5; Ferreira et al., 2015, pl. 1, fig.  
310 12) whereas other specimens appear broadly symmetric (e.g. Gardin & Manivit, 1994, pl. 3, fig. 11;  
311 Perilli & Duarte, 2006, pl. 1, fig. 9; Sandoval et al. 2012, fig. 10, n. 8-10). In both cases, the stem  
312 broadens at a different height from the base.

313 We underline that *C. cantaluppii* is often not documented or is reported with a sparse occurrence and,  
314 consequently, its biostratigraphic value remains highly questionable. In order to clarify the diagnostic  
315 features of this taxon, a detailed characterization was conducted in smear slides using four different  
316 configurations under the polarizing light microscope: with and without quartz lamina, both at 0° and  
317 45° to the polarizers (Fig. 7). Pictures at 0° to the polarizers show that specimens are rarely symmetric  
318 due to extremely variable broadening of the stem and the extremely high birefringence colors concur  
319 in suggesting that the stem broadening is due to overgrowth. Differences in asymmetry, height of  
320 stem broadening and its extension advocate variable degrees of diagenetic modifications. Indeed,  
321 pictures at 45° to the polarizers – both with and without the quartz lamina - document the overgrowth  
322 of the stem while showing the original distal shield and stem, thus allowing recognition of the original  
323 taxon.

324 *Fig. 7, about here, one column*

325 Figure 8 includes pictures of moderately and poorly (overgrown) preserved specimens of *C.*  
326 *poulnabronei*, *C. superbus* subsp. *crassus*, *C. superbus* subsp. *superbus*, *C. magharensis* subsp. *minor*  
327 and *C. magharensis* subsp. *magharensis*. The light blue bands (Fig. 8 specimens b, d, f, h) evidence  
328 overgrown specimens referable to *C. cantaluppii* of Cobianchi (1990). Specimens characterized by  
329 moderate preservation show an intermediate diagenetic phase (Fig. 8 specimens a, c, e, g, i). The use  
330 of the quartz lamina at 45° to the polarizer appears to be the best way to recognize those specimens  
331 which underwent the diagenetic modification, as in the case of photos a and b = *C. poulnabronei*, c  
332 and d = *C. superbus* subsp. *crassus*, e and f = *C. superbus* subsp. *superbus*, g and h = *C. magharensis*  
333 subsp. *minor* and i = *C. magharensis* subsp. *magharensis*.

334 *Fig. 8, about here, two columns*

335 Three diagenetic phases are separated based on the extent of overgrowth (O) starting from the base  
336 of the distal shield downwards and eventually reaching the proximal shield (Fig. 9). Phase 1  
337 characterizes specimens with negligible diagenetic modification ( $O = 0$ ). In phase 2 diagenesis affects  
338 the uppermost part of the stem without reaching the middle point of the stem ( $0 < O < SH/2$ ) (Fig. 8  
339 specimens a, c, e, g, i). In phase 3 overgrowth is more pervasive and exceeds the middle point of the  
340 stem ( $O > SH/2$ ) (Fig. 8 specimens b, d, f, h). Diagenetic modifications are generally prevalent on  
341 one side of the stem as a result of differential overgrowth producing asymmetry as in the case of the  
342 holotype of *C. cantaluppii* (Cobianchi, 1990; fig. 4, h). The species *C. cantaluppii* is, therefore, an  
343 artefact due to advanced diagenesis and not a separate taxon. In addition to taxonomic clarification,  
344 the recognition of the diagenetic phase in *Carinolithus* specimens is an effective proxy to assess the  
345 impact of overgrowth and the diagenetic degree in the studied material. In Appendix 1 we present the  
346 characterization of the diagenetic phase for all the investigated specimens illustrated in the literature.

347 *Fig. 9, about here, one column and half*

348

### 349 **4.3. Implications for the Lower and Middle Jurassic biostratigraphy**

350 The taxonomic revision of *Carinolithus* species has shown that the subsequent first occurrences (FOs)  
351 of *C. superbus* subsp. *crassus* and *C. superbus* subsp. *superbus*, have the potential to significantly  
352 increase the biostratigraphic resolution (Fig. 10).

353 The FO of *C. superbus* subsp. *crassus* has been recently identified just before the C isotopic negative  
354 anomaly associated with the T-OAE in the Sogno Core (Visentin & Erba, unpublished data; Visentin,  
355 2020). Pictures of *C. superbus* subsp. *crassus* are documented in several works (see Appendix 1) and  
356 the oldest ones (Mattioli et al., 2013; Menini et al., 2018; Da Rocha et al., 2016) derive from samples  
357 concomitant with the C isotopic positive rebound preceding the negative anomaly associated with the  
358 T-OAE. Consistent results are reported by Ferreira et al. (2019).

359 The oldest photographic documentation of *C. superbus* subsp. *superbus* (see Appendix 1) indicates a  
360 FO in the Serpentinus ammonite Zone (Baldanza & Mattioli, 1992). Ferreira et al. (2019) placed the  
361 FO of *C. superbus* “thin and long” at the Lower/Middle Toarcian boundary, in the lowermost part of  
362 the NJT7 Zone. Ongoing investigations (Visentin, 2020) confirm the FO of *C. superbus* subsp.  
363 *superbus* in the lowermost part of the NT7 Zone in the Schandelah Core from the Boreal Realm  
364 (Visentin, 2020).

365 The FO of *C. superbus* subsp. *crassus* is, therefore, older than that of *C. superbus* subsp. *superbus*  
366 and corresponds to the FO of *C. superbus* in the biozonations of Mattioli & Erba (1999) and Bown  
367 & Cooper (1998) used to define the base of the NJT6 and NJ6 Zones, respectively. Based on our  
368 taxonomic revision, the FO of *C. superbus* subsp. *crassus* should be considered the marker for the  
369 base of the NJT6 and NJ6 Zones.

370 As far as the FOs of *C. magharensis* subsp. *minor* and *C. magharensis* subsp. *magharensis* are  
371 concerned, these two taxa have been grouped together until now, so future investigations are needed  
372 to discriminate their respective first appearance level. However, *C. magharensis* subsp. *minor* and *C.*  
373 *magharensis* subsp. *magharensis*, although very rare after their first occurrence, co-occur in samples  
374 from the Lower Aalenian (base *Opalinum* Zone) of the Cabo Mondego section. However, *C.*  
375 *magharensis* subsp. *magharensis* became more common from the Bajocian upwards in Portugal.

376 *Fig. 10, about here, one column*

377

#### 378 **4.4. Evolution of the genus *Carinolithus***

379 During the Late Pliensbachian – Early Toarcian time interval, calcareous nannoplankton underwent  
380 an intense phase of diversification evidenced by the appearance of several species and genera  
381 (Mattioli & Erba, 1999; Bown et al., 2004; Erba, 2004; 2006; Menini et al., 2018). As previously  
382 discussed by Crux (1987), Bown (1987b) and Mattioli (1996), the genus *Calyculus* gave rise to the  
383 genus *Carinolithus*. Mattioli (1996; fig. 3) illustrated the transition between *Calyculus* spp. and *C.*  
384 *poulnabronei* characterized by the gradual closing of the axial canal and the development of a vertical

385 stem showing progressive thinning along with thickening of the distal shield. The hypothesis that *C.*  
386 *cantaluppii* descended from *C. poulnabronei* is here rejected since the former species, as  
387 aforementioned, represents a diagenetic artefact due to overgrowth. Therefore, *C. poulnabronei*  
388 passes to *C. superbus* subsp. *crassus* through a decrease of both shield width and thinning of the stem.  
389 Thus, in the Early Toarcian the V-shape of both the stem and the axial canal of *C. poulnabronei*  
390 coexisted with the typical T-shape of *C. superbus* subsp. *crassus*. A further decrease of the stem  
391 width characterizes *C. superbus* subsp. *superbus*, that is generally represented by taller specimens  
392 (Fig. 5). The transition between the *C. superbus* group and the *C. magharensis* group seems related  
393 to variations in thickness and ultrastructure of the distal shield. In fact, morphometry evidenced a  
394 progressive thickening of the distal shield (TDS) correlated to TH and DS ( $r = 0.66$  and  $0.64$ ,  
395 respectively) passing from *C. superbus* subsp. *superbus* to *C. magharensis* subsp. *minor*. A further  
396 increase of the DS diameter characterizes the transition from *C. magharensis* subsp. *minor* to *C.*  
397 *magharensis* subsp. *magharensis* directly correlated to an increase of PS and SW ( $r = 0.80$  and  $0.87$ ,  
398 respectively).

399

## 400 **5. Conclusions**

401 Morphometric investigations of the genus *Carinolithus* resulted in a revision of its taxonomy.  
402 Statistical treatment of the measurements validated the significance of the proposed coccolith  
403 parameters to separate taxa between and within the *C. superbus* and *C. magharensis* groups.  
404 Specifically, based on the stem width, as well as thickness and width of the distal shield two new  
405 subspecies, *C. superbus* subsp. *crassus* and *C. magharensis* subsp. *minor*, were established.  
406 The qualitative characterization of overgrowth affecting *Carinolithus* coccoliths revealed that *C.*  
407 *cantaluppii* represents a diagenetic artefact. The use of the lamina at  $45^\circ$  to the polarizers turned out  
408 to be an excellent tool to recognize the real species which underwent the diagenetic modification, and  
409 three diagenetic phases were distinguished. Overgrowth generally starts in the uppermost part of the



410 coccoliths at the base of the distal shield. Identification of the diagenetic phases can be used to  
411 evaluate nannofossil/sediment preservation and degree of secondary modifications.

412 The application of the revised taxonomy implies a revised evolution of the genus *Carinolithus* and a  
413 higher resolution of calcareous nannofossil biostratigraphy in the Toarcian and Lower Aalenian  
414 interval. In particular, the FO of *C. superbis* subsp. *superbis*, which approximates the Lower/Middle  
415 Toarcian boundary, has been recently used as an additional event in zonal schemes.

416

#### 417 **Acknowledgements**

418 The authors are grateful to the Editor Richard Jordan and two anonymous Reviewers, whose  
419 comments improved the quality of the manuscript. The research was conducted within the PRIN  
420 2017RX9XXXYY awarded to EE.

421

#### 422 **References**

423 Aguado, R., O'Dogherty, L., Sandoval, J., 2008. Fertility changes in surface waters during the  
424 Aalenian (mid-Jurassic) of the Western Tethys as revealed by calcareous nannofossils and  
425 carbon-cycle perturbations. *Marine Micropaleontology*. 68, 268-285.

426 Aguado, R., O'Dogherty, L., Sandoval, J., 2017. Calcareous nannofossil assemblage turnover in  
427 response to the Early Bajocian (Middle Jurassic) palaeoenvironmental changes in the Subbetic  
428 Basin. *Palaeogeography, Palaeoclimatology, Palaeoecology*. 472, 128-145.

429 Baldanza, A., Mattioli, E., 1992. Biostratigraphical synthesis of nannofossils in the Early Middle  
430 Jurassic of southern Tethys. *Knihovnička ZPN*. 14a (1), 111-141.

431 Bodin, S., Mattioli, E., Fröhlich, S., Marshall, J.D., Boutib, L., Lahsini, S., Redfern, J., 2010. Toarcian  
432 carbonate isotope shifts and nutrient changes from the Northern margin of Gondwana (High  
433 Atlas, Morocco, Jurassic): Palaeoenvironmental implications. *Palaeogeography,  
434 Palaeoclimatology, Palaeoecology*. 297, 377-390.

- 435 Bown, P. R., 1987a. Taxonomy, evolution, and biostratigraphy of Late Triassic-Early Jurassic  
436 calcareous nannofossils. *Palaeontological Association, Special papers in Palaeontology*. 38,  
437 1-118.
- 438 Bown, P.R., 1987b. The structural development of early Mesozoic coccoliths and its evolutionary  
439 and taxonomic significance. *Abhandlungen der Geologisches Bundesanstalt in Wien - A*, 39,  
440 33-49.
- 441 Bown, P.R., Cooper, M.K.E., Lord, A.R., 1988. A Calcareous Nannofossil Biozonation Scheme for  
442 the early to mid-Mesozoic. *Newsletter on Stratigraphy*. 20, 91-114.
- 443 Bown, P.R., & Copper, M.K.E., 1998. Jurassic. In: Bown P.R. (Ed.), *Calcareous nannofossil*  
444 *biostratigraphy*. British Micropaleontology Society Published Series: 34-85. Kluwer  
445 Academic Publishers, London.
- 446 Bown, P.R., Young, J., 1998. Techniques. In: Bown P.R. (Ed.), *Calcareous nannofossil*  
447 *biostratigraphy*. British Micropaleontological Society Published Series: 16-27. Kluwer  
448 Academic Publishers, London.
- 449 Bown, P.R., Lees, J.A., Young, J.R., 2004. Calcareous nannoplankton evolution and diversity through  
450 time. In: Thierstein H.R., Young J.R. (Eds), *Coccolithophores: from molecular processes to*  
451 *global impact*: 481-508. Springer, Berlin, Heidelberg.
- 452 Casellato, C.E., Erba, E., 2015. Calcareous nannofossil biostratigraphy and paleoceanography of the  
453 Toarcian Oceanic Anoxic event at Colle di Sogno (southern Alps, northern Italy). *Rivista*  
454 *Italiana di Paleontologia e Stratigrafia*. 121, 297-327.
- 455 Cobianchi, M., 1990. Calcareous nannofossil biostratigraphy of the Domerian-Toarcian Boundary in  
456 the Navezze Valley (Brescia). *Atti Ticinensi di Scienze della Terra*. 33, 127-142.
- 457 Cobianchi, M., 1992. Sinemurian-Early Bajocian calcareous nannofossil biostratigraphy of the  
458 Lombardy Basin (Southern calcareous Alps; Northern Italy). *Atti Ticinensi di Scienze della*  
459 *Terra*. 35, 61-106.

- 460 Crux, J.A., 1987. Concerning dimorphism in Early Jurassic coccoliths and the origin of the  
461 genus *Discorhabdus* Noël 1965. *Abhandlungen der Geologischen Bundesanstalt*. 39, 51-55.
- 462 Da Rocha, R.B., Mattioli, E., Duarte, L., Pittet, B., Elmi, S., Mouterde, R., Cabral, M.C., Comas-  
463 Rengifo, M., Gomez, J., Goy, A., Hesselbo, S., Jenkyns, H., Littler, K., Mailliot, S., Veiga de  
464 Oliveira, L.C., Osete, M.L., Perilli, N., Pinto, S., Ruget, C., Suan, G., 2016. Base of the  
465 Toarcian Stage of the Lower Jurassic defined by the Global Boundary Stratotype Section and  
466 Point (GSSP) at the Peniche section (Portugal). *Episodes Journal of International Geoscience*,  
467 Seoul National University. 39 (3), 459-481.
- 468 Deflandre, G., Fert, C., 1954. Observations sur les coccolithophoridés actuels et fossiles en  
469 microscopie ordinaire et électronique. *Annales de Paléontologie*. 40, 115-176.
- 470 Erba, E., 2004. Calcareous nanofossils and Mesozoic oceanic anoxic events. *Marine*  
471 *Micropaleontology*. 52, 85 -106.
- 472 Erba, E., 2006. The first 150 million years history of calcareous nanoplankton: Biosphere –  
473 Geosphere interaction. *Palaeogeography, Palaeoclimatology, Palaeoecology*. 232, 237-250.
- 474 Ferreira, J., Mattioli, E., Pittet, B., Cachao, M., Spangenberg, J.E., 2015. Palaeocological insights on  
475 Toarcian and Lower Aalenian calcareous nanofossils from the Lusitanian Basin (Portugal).  
476 *Palaeogeography, Palaeoclimatology, Palaeoecology*. 436, 245-262.
- 477 Ferreira, J., Mattioli, E., Suchéras-Marx, B., Giraud, F., Duarte, L. V., Pittet, B., Suan G., Hassler A.,  
478 Spangenberg, J. E., 2019. Western Tethys Early and Middle Jurassic calcareous nanofossil  
479 biostratigraphy. *Earth-Science Reviews*. 197, 1-19.
- 480 Fraguas, A., Comas-Rengifo, M.J., Perilli, N., 2015. Calcareous nanofossil biostratigraphy of the  
481 Lower Jurassic in the Cantabrian Range (Northern Spain). *Newsletter on Stratigraphy*. 48, 179-  
482 199.
- 483 Gardin, S., Manivit, H., 1994. Biostratigraphie des nanofossiles calcaires du Toarcien du Quercy  
484 (Sud-Ouest de la France). Comparisone avec la coupe stratotypique de la cimenterie  
485 d'Airvault (Deux Sevrès, France). *Geobios, M.S.* 17, 229-244.

486 Geisen, M., Bollmann, J., Herrle, J.O., Mutterlose, J., Young, J. R., 1999. Calibration of the random  
487 settling technique for calculation of absolute abundances of calcareous nannoplankton.  
488 *Micropaleontology*. 45, 437-442.

489 Grün, W., Prins, P., Zweili, F., 1974. Coccolithophoriden aus dem Lias epsilon von Holzmaden  
490 (Deutschland). *Neues Jahrbuch für Geologie und Paläontologie Abhandlungen*. 147, 294-328.

491 Hammer, Ø., Harper, D.A.T., 2006. *Paleontological Data Analysis*. Blackwell, London.

492 Hammer, Ø., Harper, D.A.T., Ryan, P.D., 2001. PAST: palaeontological statistics software package  
493 for education and data analysis. *Palaeontologia Electronica*. 4 (1), 4-9.

494 Mattioli, E., 1996. New calcareous nannofossil species from the Early Jurassic of Tethys. *Rivista*  
495 *Italiana di Paleontologia e Stratigrafia*. 102, 397-412.

496 Mattioli, E., Erba, E., 1999. Synthesis of calcareous nannofossil events in tethyan Lower and Middle  
497 Jurassic successions. *Rivista Italiana di Paleontologia e Stratigrafia*. 105, 343-376.

498 Mattioli, E., Pittet, B., Bucefalo Palliani, R., Rohl, H.J., Schimid-Rohl, A., Morettini, E., 2004.  
499 Phytoplankton evidence for the timing and correlation of paleoceanographical changes during  
500 the early Toarcian oceanic anoxic event (Early Jurassic). *Journal of Geological Society of*  
501 *London*. 161, 685-693.

502 Mattioli, E., Plancq, J., Boussaha, M., Duarte, L.V., Pittet, B., 2013. Calcareous nannofossil  
503 biostratigraphy: new data from the Lower Jurassic of the Lusitanian Basin. *Comunicações*  
504 *Geológicas. Especial I*, 69-76.

505 Medd, A.W., 1979. The Upper Jurassic coccoliths from the Haddenham and Gamlingay boreholes  
506 (Cambridgeshire, England). *Eclogae Geologicae Helvetiae*, 72 (1), 19-109.

507 Menini, A., Mattioli, E., Spangenberg, J. E., Pittet, B., Guillaume, S., 2018. New calcareous  
508 nannofossil and carbon isotope data for the Pliensbachian/Toarcian boundary (Early Jurassic)  
509 in the western Tethys and their paleoenvironmental implications. *Newsletter on Stratigraphy*.  
510 52 (2), 173-196.

511 Molina, J. M., Reolid, M., Mattioli, E., 2018. Thin shelled bivalve buildup of the lower Bajocian,  
512 South Iberian paleomargin: development of opportunists after oceanic perturbations. *Facies*.  
513 64, 19-36.

514 Moshkovitz, S., Ehrlich, A., 1976. Distribution of Middle and Upper Jurassic calcareous nannofossils  
515 in the northeastern Negev, Israel and in Gebel Maghara, northern Sinai. *Bulletin of the*  
516 *Geological Survey of Israel*. 69, 1-47.

517 Perilli, N., Duarte, L.V., 2006. Toarcian nannobiohorizons from the Lusitanian Basin (Portugal) and  
518 their calibration against ammonite Zones. *Rivista Italiana di Paleontologia e Stratigrafia* 112,  
519 417-434.

520 Reolid, M., Mattioli, E., Nieto, L.M., Rodriguez-Tovar, F.J., 2014. The Early Toarcian Oceanic  
521 Anoxic Event in the External Subbetic (Southiberian Paleomargin, Westernmost Tethys):  
522 geochemistry, nannofossils and ichnology. *Palaeogeography, Palaeoclimatology,*  
523 *Palaeoecology*. 411, 79-94.

524 Sandoval, J., Markus, B., Aguado, R., O' Dogherty, L., Rivas, P., Morard, A., Guex, J., 2012. The  
525 Toarcian in the Subbetic basin (southern Spain): Bio-events (ammonite and calcareous  
526 nannofossils) and carbonate-isotope stratigraphy. *Palaeogeography, Palaeoclimatology,*  
527 *Palaeoecology*. 342-343, 40-62.

528 Van de Schootbrugge, B., Richoz, S., Pross, J., Luppold, F.W., Hunze, S., Wonik, T., Blau, J.,  
529 Meister, C., Van de Meijst, C. M. H., Suan, G., Fraguas, A., Fiebig, J., Herrle, J.O., Guex, J.,  
530 Little, C.T.S., Wignall, P.B., Püttmann, W., Oschmann, W., 2018. The Schandelah Scientific  
531 Drilling Project: A 25-million-year record of Early Jurassic palaeoenvironmental change from  
532 northern Germany. *Newsletter on Stratigraphy*. 52 (3), 249 – 296.

533 Visentin, S., 2020. Calcareous nannofossil biostratigraphy and taxonomy across the Early Toarcian  
534 Oceanic Anoxic Event: a comparison between Tethyan and Boreal sections. Ph.D. thesis,  
535 Department of Earth Sciences “Ardito Desio”. University of Milan, Italy.

536

CAPTIONS

537  
538  
539  
540  
541  
542  
543  
544  
545  
546  
547  
548  
549  
550  
551  
552  
553  
554  
555  
556  
557  
558  
559  
560  
561  
562

**Fig. 1.** Holotypes of *R. superbus* (Deflandre in Deflandre & Fert, 1954) (a), *R. sceptrum* (Deflandre in Deflandre & Fert, 1954) (b), *R. clavatus* (Deflandre in Deflandre & Fert, 1954) (c), *H. magharensis* (Moshkovitz & Ehrlich, 1976) (d), *C. cantaluppii* (Cobianchi, 1990) (e) and *C. poul nabronei* (Mattioli, 1996) (f).

**Fig. 2.** Synthesis of the morphometric analyses performed on the *C. superbus* (in blue) and *C. magharensis* (in red) groups. Total height, stem height, stem width, proximal shield diameter, distal shield diameter and thickness of distal shield are indicated. The number of specimens measured (N) for each parameter is indicated.

**Fig. 3.** Correlation plots of the measured parameters. Every parameter is compared with each other. For each scatter plot, the Pearson's correlation coefficients (r), the linear regression line, the number of measured specimens (N) are given. Note that for TDS/SW, TDS/SH, TDS/PS, TDS/TH and TDS/DS the two groups are confined to clearly separated and distinct sets that do not overlap.

**Fig. 4.** Distribution histograms for a) the distal shield diameter (histogram class sizes 0.5  $\mu\text{m}$ ), b) thickness of the distal shield (histogram class sizes 0.2  $\mu\text{m}$ ) and c) stem width (histogram class sizes 0.2  $\mu\text{m}$ ). Histograms provide the number of data for each size bin, highlighting differences in morphology.

**Fig. 5.** Summary of sizes of investigated parameters in the holotypes and the variability quantified for the measured specimens for individual *Carinolithus* taxa. Number of specimens measured (N) are provided for each parameter.

563 **Fig. 6.** Photographs documenting the revised taxonomy. A = *C. superbus* subsp. *crassus* (a-f); B = *C.*  
564 *superbus* subsp. *superbus* (g-l), C = *C. magharensis* subsp. *minor* (m-r), D = *C. magharensis* subsp.  
565 *magharensis* (s-x). Specimens a, b, g, h, i, j, k, l, m, n, o, p, s, t are from this work: (a, b) Sogno Core;  
566 (g, h, i, j, k, l, m, n, o, p, s, t) Breggia section. Specimens c, d, e, f, q, r, u, v, w, x are from literature:  
567 (c) Bown & Cooper (1998; pl. 4.13, fig. 11); (d) Bown (1987a; pl. 14, fig. 15); (e) Menini et al. (2018;  
568 pl. 1, fig. 33); (f) Van de Schootbrugge et al. (2018; pl. 6, fig. 11); (q) Bown (1987a; pl. 14, fig. 17);  
569 (r) Bown & Cooper (1998; pl. 4.13, fig. 8); (u) Aguado et al. (2017; fig. 8, y); (v) Aguado et al. (2008;  
570 fig. 5, n. 19); (w) Bown & Cooper (1998; pl. 4.13, fig. 6); (x) Bown & Cooper (1998; pl. 4.13, fig.  
571 7).

572

573 **Fig. 7.** Specimens of *C. cantaluppii* photographed in four different combinations both with and  
574 without quartz lamina, at 0° and 45° to the polarizers. Illustrated specimens are from the Breggia  
575 section.

576

577 **Fig. 8.** Photographs of *Carinolithus* specimens investigated in this study and taken from the literature.  
578 Specimens investigated in this study are illustrated with and without quartz lamina, at 0° and 45°  
579 relative to the polarizers. Based on the description proposed by Cobianchi (1990) specimens  
580 highlighted with light blue rectangles were assigned to *C. cantaluppii* before the current taxonomic  
581 revision. The new taxonomic identification of *Carinolithus* specimens allows to distinguish the true  
582 taxon which underwent diagenetic modifications. (a1-a4, b1-b4, c1-c4, d1-d4) Sogno Core; (e1-e4,  
583 f1-f4, g1-g4, h1-h4, i1-i4) Breggia section; (a5, a6) Sandoval et al. (2012; fig. 10, n. 16, 17); (b5, b6,  
584 b7) Mattioli (1996; pl. 2, figs. 9,11,12); (c5) Menini et al. (2018; pl. 1, fig. 33); (c6) Casellato & Erba  
585 (2015; pl. 1, fig. 16); (c7) Van de Schootbrugge et al. (2018; pl. 6, fig. 11); (d5) Reolid et al. (2014;  
586 fig. 6, CE30); (d6) Bodin et al. (2010; fig. 5, i); (e5) Sandoval et al. (2012; fig.10, n. 20); (e6) Sandoval  
587 et al. (2012; fig. 10, n. 12); (e7) Aguado et al. (2008; fig. 5, n. 18); (e8) Molina et al. (2018; fig. 8,  
588 LL6); (f5) Ferreira et al. (2015; pl. 1, fig. 12); (f6) Cobianchi (1990; fig. 4, h) ; (g5) Sandoval et al.

589 (2012; fig. 10, n. 19); (g6) Bown & Cooper (1998; pl. 4.13, fig. 8); (g7) Bown (1987a; pl. 14, fig.  
590 17); (i5) Aguado et al. (2008; fig. 5, n. 19); (i6) Bown & Cooper (1998; pl. 4.13, fig. 6).

591

592 **Fig. 9.** Schematic representation of increasing diagenetic phases of *Carinolithus* specimens: SH =  
593 stem height; SH/2 = half the stem height; O = overgrowth. **Phase 1:** no or negligible diagenetic  
594 overprint (O = 0); **Phase 2:** overgrowth affects the uppermost part of the stem, starting from the base  
595 of the distal shield downwards without reaching the stem middle point ( $0 < O < SH/2$ ); **Phase 3:**  
596 diagenesis becomes more pervasive and exceeds the middle point of the stem ( $O > SH/2$ ). Overgrowth  
597 may affect one or both sides of the stem and with different degrees.

598

599 **Fig. 10.** Stratigraphic distribution of *C. poul nabronei*, *C. superbis* subsp. *crassus* and *C. superbis*  
600 subsp. *superbus*.

601

602 **Tab. 1.** Number of specimens, mean, median, mode and standard deviation of measured taxonomic  
603 characters (TH, SH, SW, PS, DS, TDS): a) all specimens; b) *C. magharensis* group; c) *C. superbis*  
604 group.

605

606 **Appendix 1** – Data – set of *Carinolithus* specimens from literature used for morphometric analyses.  
607 Data are organized following the publication date and for each specimen the following information  
608 is given: investigated core/section; nomenclature adopted in the original paper; revised nomenclature  
609 following the revised taxonomy (this study); stage/substage; ammonite and calcareous nannofossil  
610 Zones and Subzones. Specimens selected for morphometric analyses are characterized with an X. The  
611 other specimens were used to characterize the diagenetic overprint. *Carinolithus* \* is reported for  
612 specimens not attributable to a species due to high overgrowth.

613

614



615  
616  
617  
618  
619  
620  
621  
622  
623  
624  
625  
626  
627  
628  
629  
630  
631  
632  
633  
634  
635  
636

FIGURES

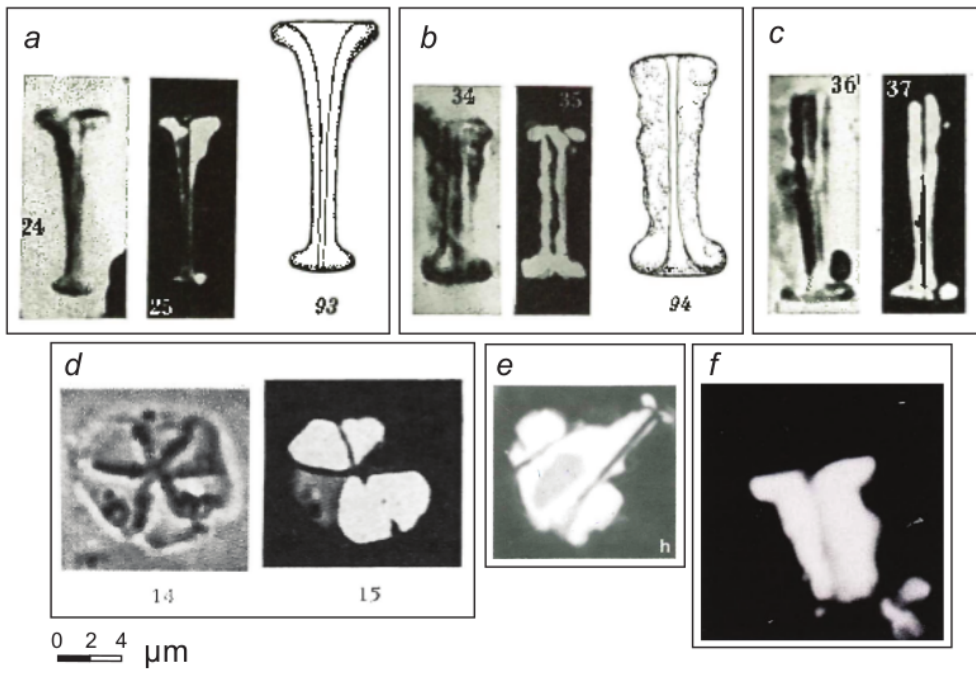
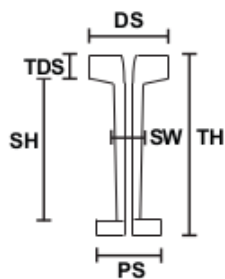
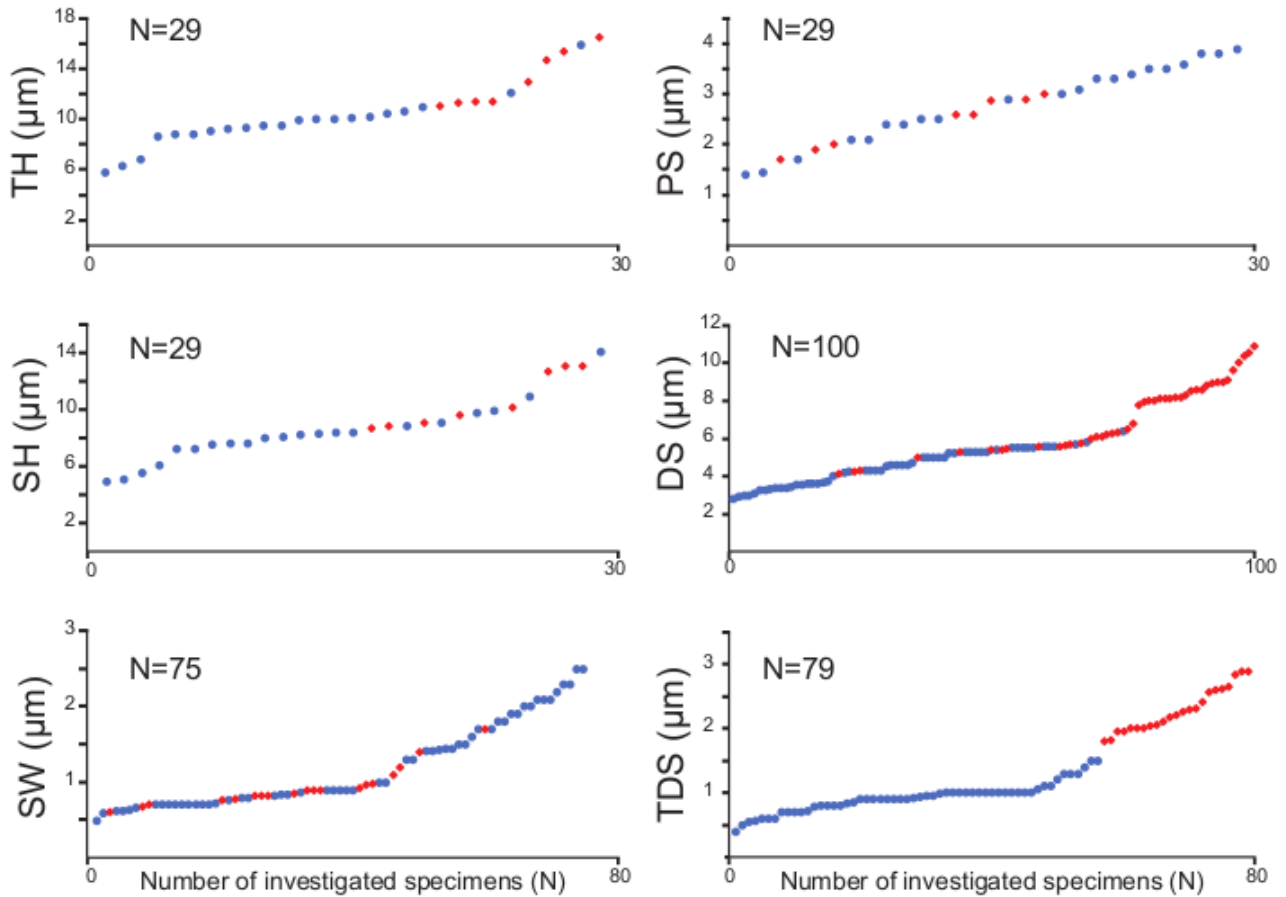


FIG. 1.PDF (one column and half) NOT COLOURS



**TH**: Total Height  
**SH**: Stem Height  
**SW**: Stem Width  
**PS**: Proximal Shield diameter  
**DS**: Distal Shield diameter  
**TDS**: Thickness of Distal Shield

● *C. superbis* group  
 ◆ *C. magharensis* group

637

638

639

640

641

642

643

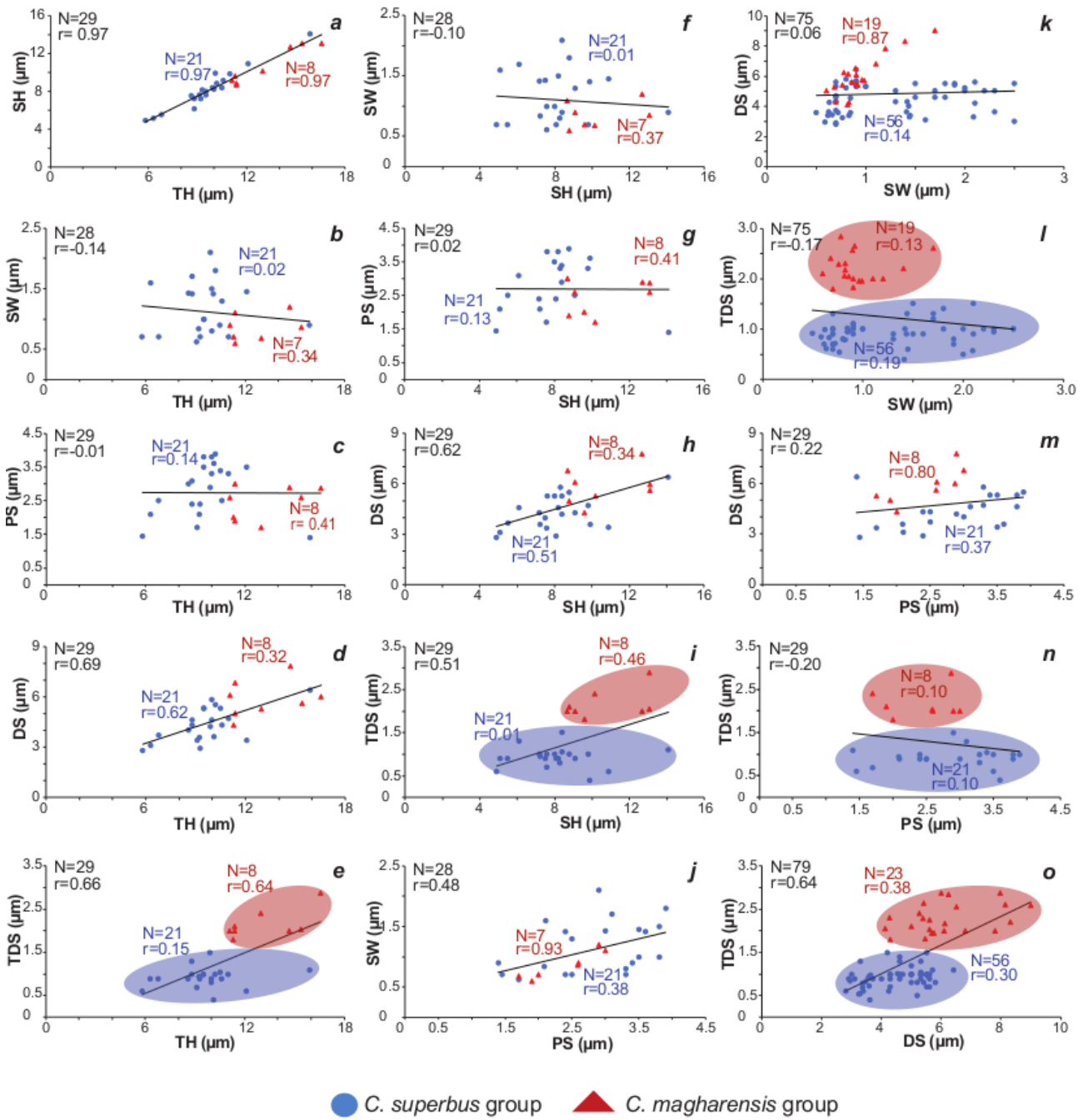
644

645

646

647

FIG. 2.PDF (two columns) COLOURS



649

650

651

FIG. 3.PDF (two columns) COLOURS

652  
653  
654  
655  
656  
657  
658  
659  
660  
661  
662  
663  
664  
665  
666  
667  
668  
669  
670  
671  
672  
673  
674  
675  
676  
677  
678  
679

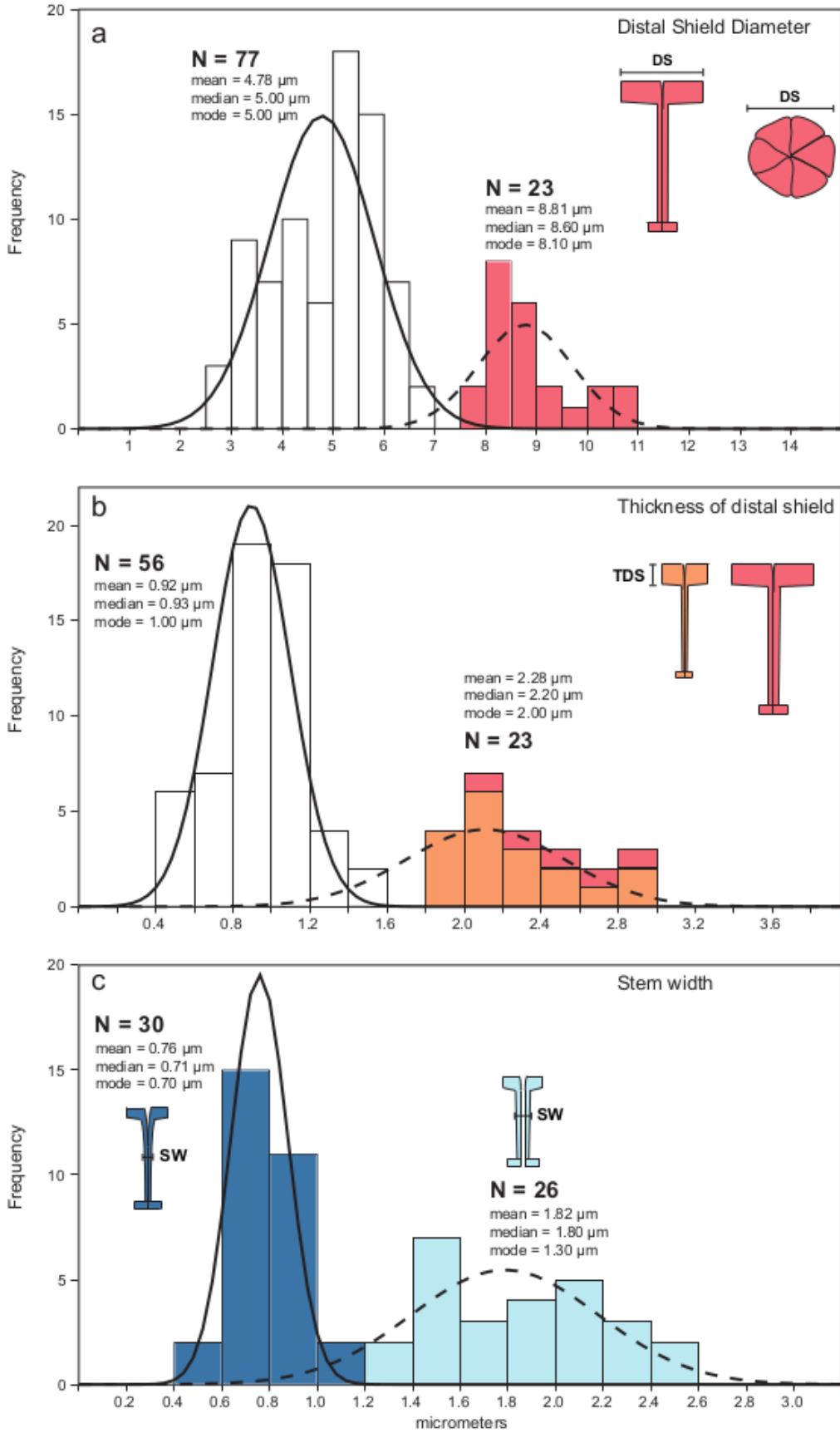


FIG. 4.PDF (two columns) COLOURS

680  
681  
682  
683  
684  
685  
686  
687  
688  
689  
690  
691  
692  
693  
694  
695  
696  
697  
698  
699  
700  
701  
702  
703  
704  
705  
706  
707

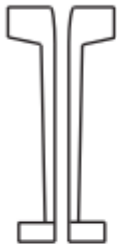


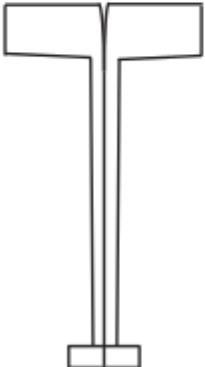
		TH	SH	SW	PS	DS	TDS
<i>C. superbus</i> subsp. <i>crassus</i>		Holotype					
		8.8	6.1	1.7	3.1	4.6	1.3
		Variability among investigated specimens					
		N=10 6.3 - 12.1	N=10 5.1 - 10.9	N=26 1.3 - 2.5	N=10 2.1 - 3.9	N=26 3.0 - 5.6	N=26 0.4 - 1.5
<i>C. superbus</i> subsp. <i>superbus</i>		Holotype					
		10.3	8.5	0.7	2.7	4.3	1.0
		Variability among investigated specimens					
		N=11 5.8 - 15.9	N=11 4.9 - 14.1	N=30 0.5 - 1.0	N=11 1.4 - 3.9	N=30 2.8 - 5.8	N=30 0.5 - 1.3
<i>C. magharensis</i> subsp. <i>minor</i>		Holotype					
		/	/	/	/	5.6	2.3
		Variability among investigated specimens					
		N=7 11.1-16.6	N=7 8.7 - 13.1	N=16 0.6 - 1.1	N=7 1.7 - 3.0	N=21 4.1 - 6.8	N=18 1.8 - 2.9
<i>C. magharensis</i> subsp. <i>magharensis</i>		Holotype					
		/	/	/	/	8-9	/
		Variability among investigated specimens					
		N=1 /	N=1 /	N=3 1.2 - 1.7	N=1 /	N=23 7.8 - 10.9	N=5 2.0 - 2.9

FIG. 5.PDF (one column and half) NOT COLOURS

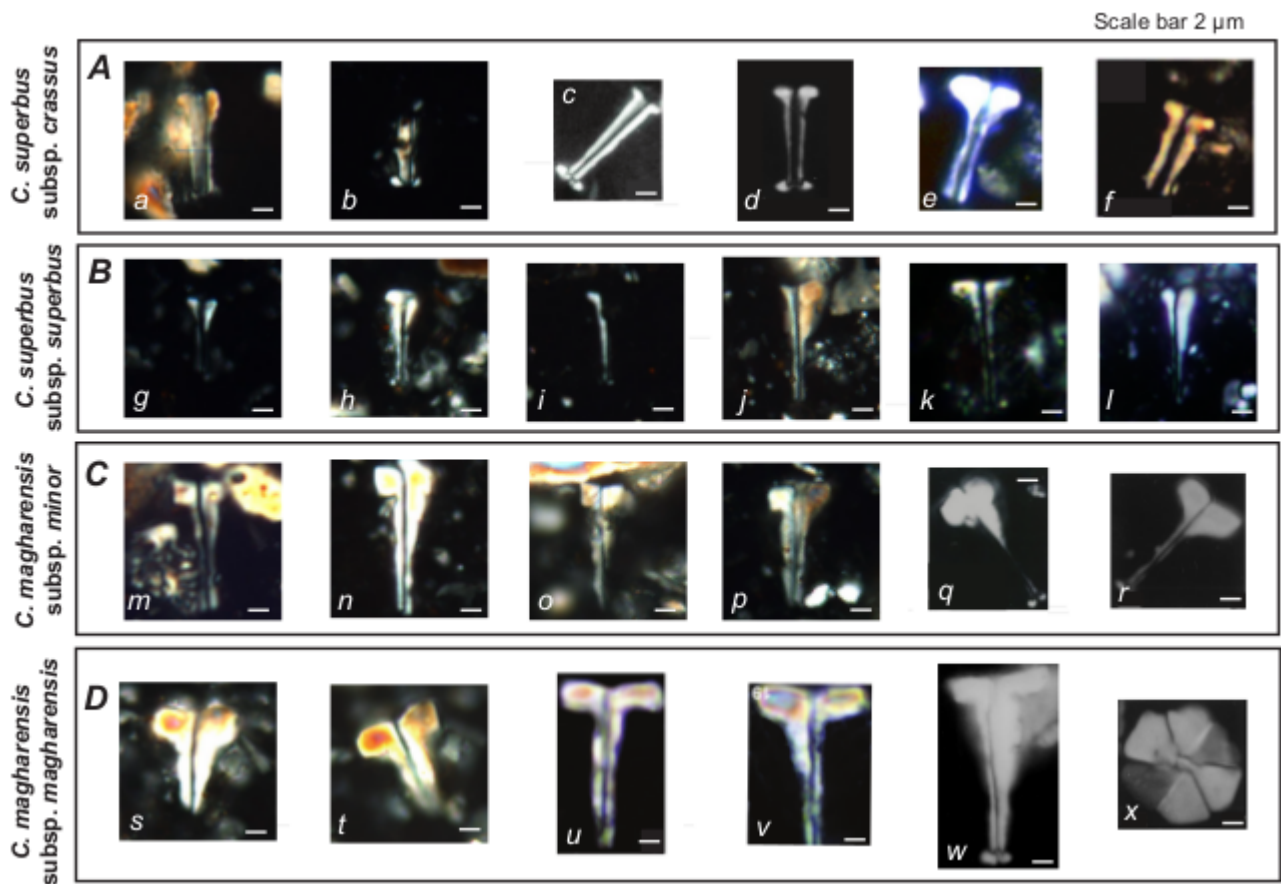


FIG. 6.PDF (two columns) COLOURS

709

710

711

712

713

714

715

716

717

718

719

720

721

722

723  
724  
725  
726  
727  
728  
729  
730  
731  
732  
733  
734  
735  
736  
737  
738  
739  
740  
741  
742  
743  
744  
745  
746

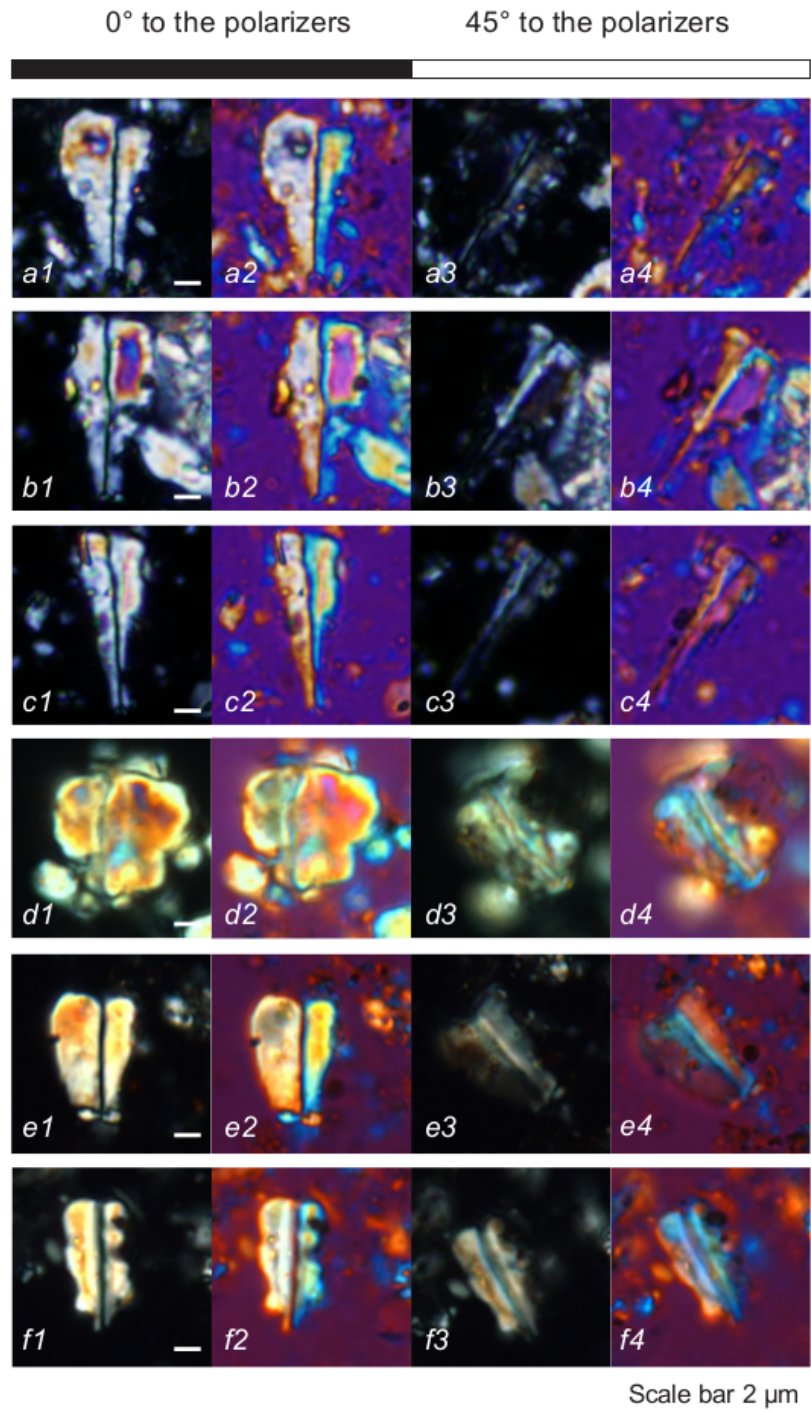


FIG. 7.PDF (one column) COLOURS

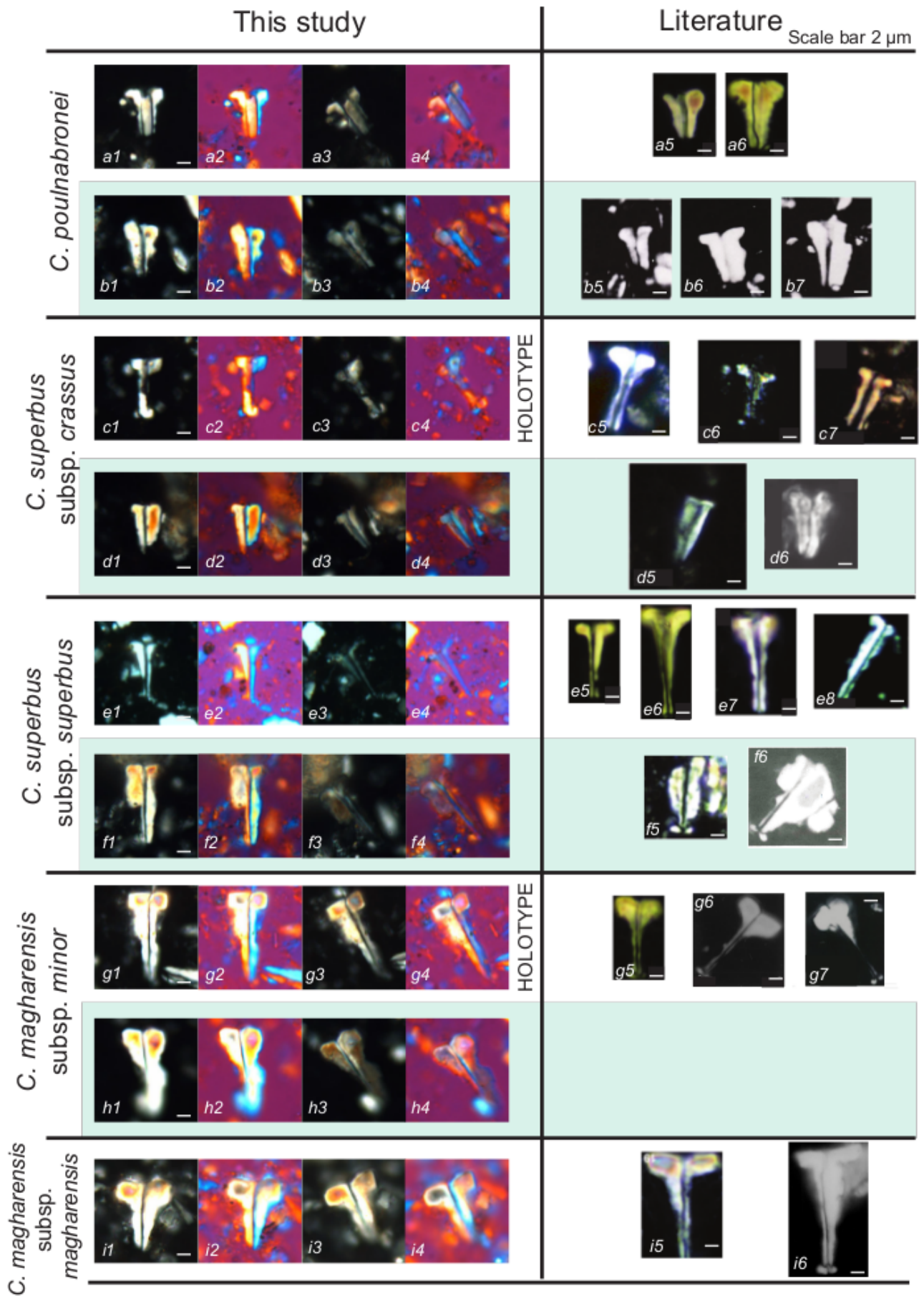


FIG. 8.PDF (two columns) COLOURS



748

749

750

751

752

753

754

755

756

757

758

759

760

761

762

763

764

765

766

767

768

769

770

771

772

773

774

775

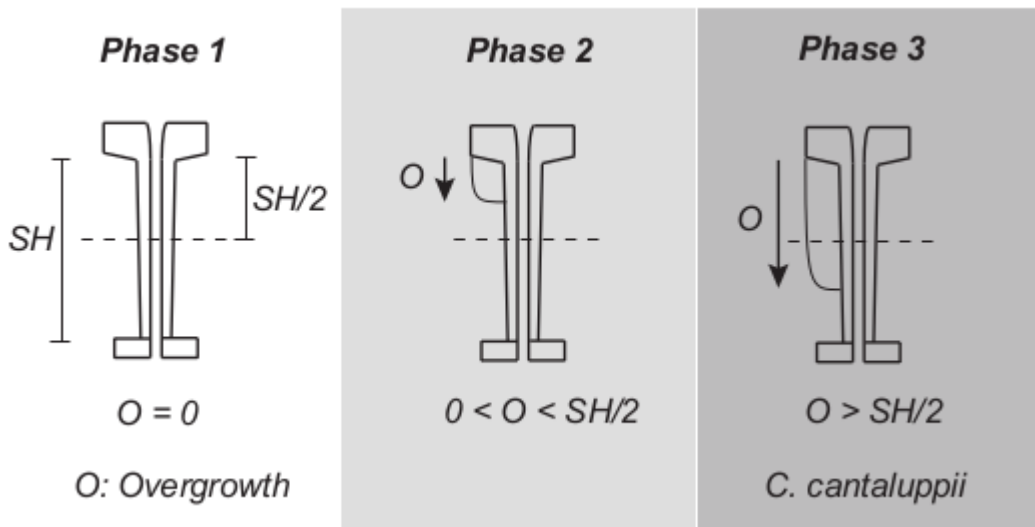


FIG. 9.PDF (one column and half) NOT COLOURS

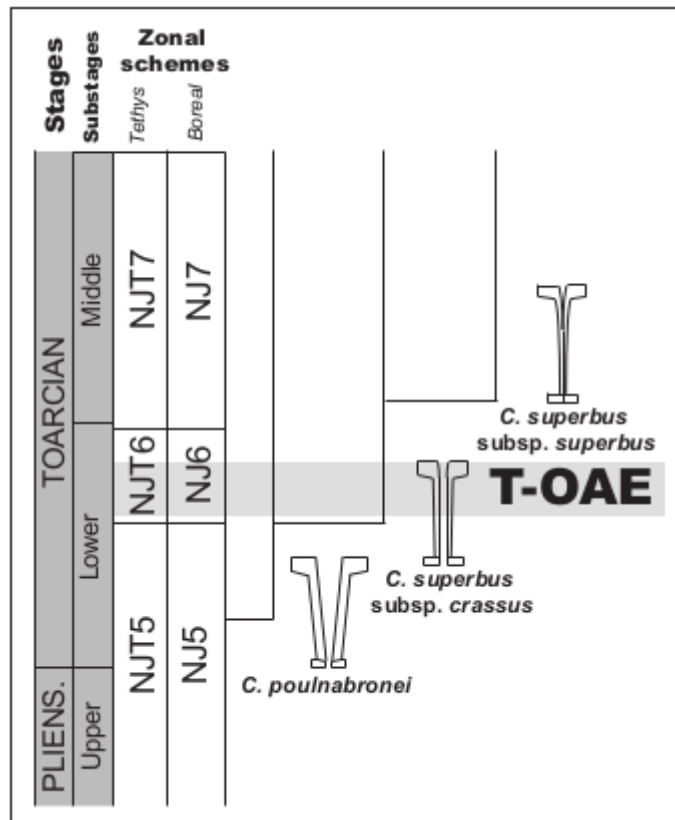


FIG10.PDF (one column) NOT COLOURS

TABLE 1. (one column and half)

	<b>TH</b>	<b>SH</b>	<b>SW</b>	<b>PS</b>	<b>DS</b>	<b>TDS</b>
<b>a. Total specimens</b>						
<b>Number of specimens</b>	29	29	75	29	100	79
<b>Mode</b>	8.80	8.40	0.70	1.70	5.00	1.00
<b>Median</b>	10.20	8.40	0.90	2.87	5.40	1.00
<b>Mean</b>	10.59	8.82	1.17	2.73	5.71	1.32
<b>Standard deviation</b>	2.60	2.29	0.55	0.73	1.97	0.67
<b>b. <i>Carinolithus magharensis</i> group</b>						
<b>Number of specimens</b>	8	8	19	8	44	23
<b>Mode</b>	11.40	/	0.90	/	8.10	2.00
<b>Median</b>	12.19	9.81	0.90	2.59	7.88	2.20
<b>Mean</b>	13.11	10.63	0.94	2.44	7.28	2.28
<b>Standard deviation</b>	2.16	1.97	0.26	0.51	1.81	0.34
<b>c. <i>Carinolithus superbus</i> group</b>						
<b>Number of specimens</b>	21	21	56	21	56	56
<b>Mode</b>	8.80	8.40	0.70	2.40	5.00	1.00
<b>Median</b>	9.50	8.10	0.95	3.00	4.60	0.93
<b>Mean</b>	9.63	8.12	1.25	2.84	4.47	0.92
<b>Standard deviation</b>	2.08	2.04	0.59	0.78	0.95	0.23